Chemosphere 275 (2021) 129935

Contents lists available at ScienceDirect

Chemosphere

journal homepage: www.elsevier.com/locate/chemosphere

Concomitant behavior of arsenic and selenium from the karst infillings materials of the fractured carbonate Dogger Aquifer (Hydrogeological Experimental Site, Poitiers, France)

R. Mhanna [a, *], A. Naveau [a], M. Bueno [b], M. Shmeit [a], F. Ismail [a], C. Fontaine [a], G. Porel [a], J. Bassil [c], L. Caner [a]

[a] Université de Poitiers, UMR 7285 IC2MP-HydrASA, TSA 51106, 5 Rue Albert Turpain, 86073, Poitiers Cedex 9, France
[b] CNRS/Univ. Pau & Pays de L'Adour/E2S UPPA, Institut des Sciences Analytiques et de Physico-Chimie pour L'Environnement et Les Matériaux (IPREM), UMR 5254, 64053, Pau, France
[c] L2GE, Lebanese University, Faculty of Sciences 2, Fanar, Matn, Lebanon

HIGHLIGHTS

- Clayey karst-infillings of the mid-Jurassic aquifer are geogenic sources of Se in the HES of Poitiers.
- Pyritic minerals were initially the main carrier of As and Se in the clayey materials.
- After pyrite oxidation, As was primarily associated with iron oxyhydroxides and Se was associated with OM.
- In acidic and basic conditions, their release is controlled by partial dissolution of the carrier phases and desorption processes, respectively.
- At circumneutral pH, As and Se exhibit different behaviors, with a higher release of Se than As.

ARTICLE INFO

Article history:
Received 11 October 2020
Received in revised form
29 January 2021
Accepted 7 February 2021
Available online 15 February 2021

Handling Editor: X. Cao

Keywords:
Arsenic
Selenium
Carbonated aquifer
Chemical extractions
Leaching

ABSTRACT

Petrographic and mineralogical analyses combined with sequential extractions and leaching experiments as a function of pH were performed on black clayey sediments fulfilling karsts in the Hydrogeological Experimental Site (HES) of Poitiers (France) to investigate the behavior of arsenic and selenium in a fractured limestone aquifer.

Sequential extractions showed that arsenic is mainly associated with pyrite (about 35%) and secondary iron oxyhydroxides (around 13%), along with a substantial exchangeable fraction (about 13%). The soluble fraction and the fraction associated to organic matter are ~2% and ~5%, respectively. The distribution of selenium is mainly pyritic (around 39%) or associated with organic matter (about 18%). Its association to secondary iron oxyhydroxides minerals is low (around 2%), whereas its soluble fraction is around 5%.

SEM analyses revealed the presence of arsenic "hot spots" into euhedral pyrite crystals surrounded by a halo of iron oxyhydroxides resulting from their alteration, and both are enriched with arsenic. Selenium has a similar pyritic origin but after alteration, it is predominantly associated with organic matter.

Despite different distributions, the leaching experiment as a function of pH showed that the mobilization of arsenic and selenium overlapped below pH 2 and above pH 8. The main differences were observed between pH 2 and 8 with a plateau at 5% of released selenium, whereas the amount of mobilized arsenic continuously decreased. The pH-dependence of both elements is attributed to the partial dissolution of pyrite in acidic conditions combined with desorption processes at higher pH values.

1. Introduction

Arsenic (As) and selenium (Se) are trace elements normally present in scarce amounts in water bodies. However, their cumulative build-up can cause detrimental effects on human health, including several types of cancer (Chen et al., 1992; Tamoto et al.,

* Corresponding author.
E-mail address: rana-mhanna@hotmail.com (R. Mhanna).

https://doi.org/10.1016/j.chemosphere.2021.129935
0045-6535/

2015). As a result, the European Union established standards at 10 μg/L in 1998 (European Union, 1998) for both elements as limits of consumption in drinking water. Both elements exist as oxyanions, and their speciation is controlled by different factors such as pH, redox conditions (Eh), water composition, and dissolved oxygen (DO) (Rosen and Liu, 2009). The inorganic species are usually more harmful than the organic ones, and the most common forms found in nature are arsenite (AsIII) and arsenate (AsV) for arsenic, and selenite (SeIV) and selenate (SeVI) for selenium (Smedley and Kinniburgh, 2002; Nakamaru and Altansuvd, 2014; Tabelin et al., 2017).

The mechanisms that control the mobility of these elements firstly depend on the solubility of the primary bearing-minerals, such as sulfides, arsenides, and selenides. The first steps of mobilization are related to dissolution/precipitation processes and/or sorption/desorption reactions (Wilkin et al., 2018). Geogenic sources of As and Se were reported in aquifers of many countries around the world (Raessler, 2018; Wilkin et al., 2018). Common secondary phases in sediments are responsible for the retention of both elements, such as carbonates, oxhydroxides, organic matter, sulfides, and clay minerals. Thus, to correctly assess the environmental behavior of the two elements, it is important to investigate their distribution and their geochemical associations in sediments, as well as their potential mobility under different environmental conditions.

Parallel and sequential extractions are simple and effective methods that provide insights into the bioavailability, mobility, carrier phases, and release mechanisms of trace elements into water bodies (Tessier et al., 1979). They have been extensively used to assess the various distribution of As and Se in different solid constituents (Bassil et al., 2016; Javed et al., 2014; Kim et al., 2014; Martens and Suarez, 1997; Wenzel et al., 2001). Javed et al. (2014) showed that arsenic was mainly present in sulfide-bearing minerals in shale deposits and specifically sorbed on the mineral and organic phases. Likewise, Kim et al. (2014) showed that arsenic was mainly retained by sulfide minerals and their weathering products, including iron oxides, in the studied soils. On the other hand, Kulp and Pratt (2004) reported that sulfide minerals, mainly pyrite, and organic compounds were the predominant carriers for selenium in organic-rich chalks and shales. Similar results obtained by Matamoros-Veloza et al. (2011) revealed that the primary hosts for Se in various shales in the world are pyrite and organic matter, but they considered that selenium had a higher affinity for pyrite at lower concentrations.

In addition to chemical extractions, the analysis of the pH effect on the leachability of As and Se helps to better identify the carrier phases and their release mechanisms into the environment (Jegadeesan et al., 2008; Tabelin et al., 2014; Tamoto et al., 2015; Wang et al., 2018).

Selective extractions and leaching experiments of previous studies in the Dogger aquifer highlighted the diversity of selenium distribution in continental sedimentary clay karst infilling material, inducing multiple release mechanisms (Bassil et al, 2016a, 2018). The presence of soluble selenium in different wells of the Hydrogeological Experimental Site (HES) of Poitiers was nevertheless mainly attributed to the relatively important easy-mobilizable Se fraction. The mobility of this fraction seemed to be mainly ruled by its association with the organic matter present in the argillaceous samples.

The groundwater from the Dogger aquifer of the HES exhibits soluble selenium concentrations ranging between 10 and 40 μg/L in different wells whereas no detectable presence of arsenic was quantified (Bassil et al., 2016a, 2018). These behaviors contrast with the chemical composition of the associated sedimentary materials, which contain about fourfold higher arsenic than selenium (Bassil et al., 2016a, 2018). Even though the karsts partially filled by clayey sediment are discontinuous in the mid-Jurassic limestone, they represent an important rock-source of As and Se at the regional scale for Dogger aquifer.

Many studies examined the leaching behaviors of arsenic and selenium concomitantly (Su and Wang, 2011; Tabelin et al., 2014; Wilkin et al., 2018b; Yang and He, 2016). However, studies with systematic comparisons between the geochemical behavior of As and Se are limited. In the present study, we focused on comparing the distribution and behavior of the two elements in dark argillaceous sediments found in karstic cavities of a mid-Jurassic aquifer. The primary objectives are: (1) performing petrographic investigations using optical microscopy, scanning electron microscope coupled with energy dispersive X-ray (SEM-EDX), and X-ray diffraction; (2) evaluating the distribution of As and Se using parallel and sequential extractions; (3) examining the effect of pH on their release; (4) correlating the occurrences of As and Se as well as the coexisting ions and geochemical parameters. Finally, all data have been statistically analyzed based on the null hypothesis i.e. by assuming that the behaviors of arsenic and selenium are different.

2. Materials and methods

2.1. Site description, sampling, and preparation

This study was carried out on the Dogger aquifer of the Hydrogeological Experimental Site (HES) of Poitiers. The HES is a research platform of the University of Poitiers and belongs to the SOERE H^+ Network (http://hplus.ore.fr/) dedicated to long-term monitoring and understanding of groundwater flow and solute transfer in heterogeneous carbonate aquifer (Audouin et al., 2008; Le Coz et al., 2017; Mari et al., 2020). The Dogger aquifer corresponds to the carbonates of Middle Jurassic age of about 100 m thick (~20—~130 m from ground level) with the presence of pervasive karstic caves and conduits (Mari et al., 2020), partially infilled by clayey sediments of various composition and color. The studied samples were collected in 2012 through non-destructive drilling at a depth between 66 m and 71 m in a borehole called C5 that crosses the Dogger aquifer of the HES. The collected samples are clayey sediments enriched in organic matter, pyrite, and selenium that fulfill a part of the karst cavities developed within the Bajocian limestone host rocks, as described by Bassil et al. (2016b). Extensive characterizations dated the selected samples from the Upper Cretaceous, and showed the external and continental origin of the infilling materials and their transformation after deposition under reducing conditions (Bassil et al., 2016b).

2.2. Instrumentation and analysis

2.2.1. Characterization of the sedimentary sample

The total elemental composition of the sample C5-BjF was determined by ICP-MS after $LiBO_2$ fusion and acid dissolution in an accredited laboratory (CRPG-CNRS, Nancy, France - http://www.crpg.cnrs-nancy.fr/SARM/index.html), by CHNS analysis (Flash, 2000 Thermo, IC2MP, France) for the organic C and total S, and by ICP-MS for total As and total Se (Agilent 7500ce, IPREM, France).

Powdered samples (infra 50 μm fraction) were analyzed by X-ray diffraction (XRD) using Phillips Panalytical X'Pert Pro apparatus in the same experimental conditions as described by Bassil et al. (2016b). The phase identifications were made with the X'pert HighScore software, while the semi-quantifications were obtained by applying the RIR method (Chung, 1975; Hillier, 2000) to major peak areas. The RIR values used for the identification are available in JCPDS Pdf2 mineralogical database. Based on experimental peaks correction using corundum (α-Al_2O_3) as an external standard, this

method is simple and efficient when clay minerals do not have specific chemical compositions and show great variabilities of peak intensities due to structural disorder (Xiang et al., 2018), which is the case for the kaolinite-rich studied samples. Diffractograms presented in Fig. 1 were normalized to the peak intensity of kaolinite at 7.19 Å.

Thin sections (26 × 46mm; 30 μm thickness) were prepared from undisturbed samples after impregnation at room temperature and under atmospheric pressure, with a two-component epoxy resin (Araldite, 2020) diluted with 20% acetone. The thin sections were observed using an optical polarized light microscope (Nikon Eclipse E600 POL) and then using a scanning electron microscope JEOL 5600-LV [Low Vacuum] (IC2MP, UP, Poitiers) equipped with a secondary electron detector Everhart – Thornley and a back-scattered electron detector Centaurus (KE Development ic, Cambridge), with a Bruker energy dispersive X-ray spectrometer for scanning electron microanalyses (SEMA). Additional pictures were obtained using a scanning electron microscope Jeol JSM-7900F. The pictures were obtained at working distances of 10 mm and an accelerating voltage of 20 kV. Data processing was provided by the chemical analysis software QUANTAX.

2.2.2. Chemical extractions

Protocol choices were based on a compromise between different classical extraction schemes developed for arsenic and selenium (Bassil et al., 2016a; Javed et al., 2013; Kim et al, 2014, 2016; Martens and Suarez, 1997; Wenzel et al., 2001; Zhang and Jr, 2003). A series of multiple parallel extractions (Table 1) were therefore tested to develop a six-step extraction protocol that targets both arsenic and selenium phases. The protocol was applied in a sequential scheme with two different contact times, described in Table 2. In addition, the release of potentially interesting elements (Fe, Mn, Ca, Mg, Al, Si, TOC) was monitored to have an insight into the possible solid phase carriers.

The sediment (C5-BjF) used in this study was preserved since 2012 at low temperature (−18°C) under an argon atmosphere. For this protocol, the sample was freeze-dried, ground into a powder with agate mortar, and then sieved at 200 μm. Solid suspensions containing 600 mg of powdered solid and 20 mL of the extraction solution were then prepared directly in centrifuge tubes to minimize the possible loss between the different steps. Tubes were closed during the extraction period and agitated at a speed of 350 rpm. Suspensions were then centrifuged for 10 min at a speed of 14,000 rpm using Thermo Scientific Heraeus biofuge stratos and then filtrated through a 0.45 μm Sartorius nylon membrane. The equilibrium pH of the supernatant was measured by a pH meter Metrohm 827 immediately after separation. Recovered supernatants were stored at 4 °C before further analysis. The next extraction solution was added to the remaining residue of each step. Solid residues obtained at the end of the sequential extractions scheme were oven-dried for 1 week at 105 °C, ground with agate mortar, and stored for mineralogical analyses. The residual fraction was calculated by subtracting the total released element during extraction, from the total concentration. All the chemical reagents used were of analytical grade. The used ultrapure water was obtained from the Milli-Q system (18.2 MΩ cm^{-1}, Elix, Millipore).

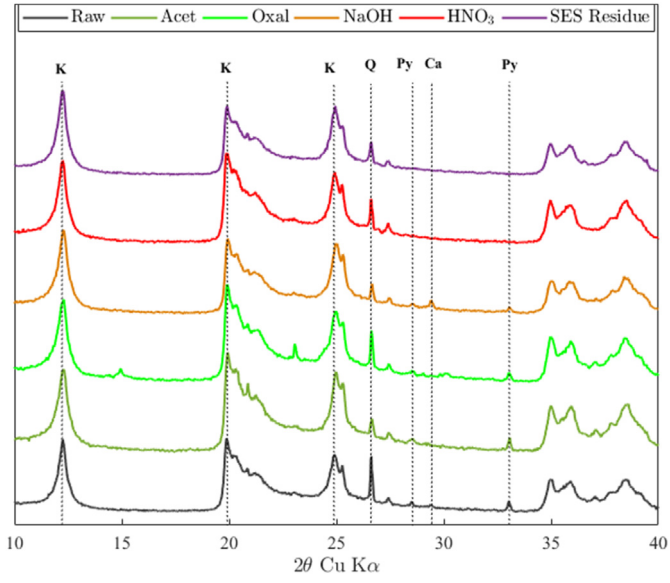

Fig. 1. X-ray diffraction patterns of the sedimentary sample C5-BjF and the residues after parallel extractions. The patterns were normalized to the intensity of the peak of kaolinite (K) that is not affected by the chemical extractions. Note the changes in the peak intensities of pyrite (Py) and calcite (Ca) with the different treatments. Q: Quartz.

2.2.3. Chemical analyses

Quantifications of As and Se in the extracted solutions were performed by ICP-MS (Agilent 7500ce, IPREM, France) with operating conditions as described by Bassil et al. (2016a) except the use of H_2–He mixture (3.5–1.5 mL min^{-1}) for the octupole collision/reaction cell. The AAS (Varian AA24FS, IC2MP, France) was used for the quantification of major elements and ICP-OES (Agilent Technologies 5110, IC2MP, France) for Si and Al. Speciation of arsenic and selenium was performed by HPLC coupled to the same ICP-MS used for total As and Se measurements. The chromatographic system consisted of an Agilent 1100 series HPLC pump, equipped with an autosampler and variable volume sample loop. The HPLC-ICPMS interface was made up of a polyetheretherketone (PEEK) tube. Chromatographic separation was carried out on anion exchange stationary phase (Agilent G3154 column 15 cm × 4.6 mm i.d.) with ammonium nitrate mobile phase (20 mmol L^{-1}, 2,5% methanol and pH 8.5 adjusted with ammonia) delivered at 1 mL min^{-1} flow rate. Selected chromatography allowed the separation of arsenite, arsenate, selenite, and selenate species.

2.2.4. Batch leaching experiments

Batch leaching experiments were performed at ambient temperature in borosilicate flasks in which suspensions were prepared by mixing the sample C5-BjF with ultrapure water during a contact time of 1 week and under agitation with a reverse system at 30 rpm. The pH was adjusted at the beginning of the experiment by the addition of 1 M NaOH or HCl and the equilibrium pH of the supernatant was measured directly after separation.

The preparation of the sedimentary sample, the SL ratio, the separation method, the storage conditions, and the quantifications of the leachates were carried out as described in part 2.2.2.

2.2.5. Statistical studies

The statistical analyses were performed using R studio. Correlation coefficients were calculated using Pearson's method with a confidence interval of 5%. Correlation tables related were performed with 6 reagents and 6 parameters for extraction experiments and 12 acid/base conditions and 6 or 9 parameters for leaching experiments.

3. Results and discussion

3.1. Chemical, mineralogical and petrographical characterizations

The karst infilling material C5-BJF is composed of a clayey matrix (mainly kaolinite and smectite to a lesser extent) with traces of

Table 1
Experimental conditions of the single parallel extractions.

Code	Reagent	Concentration	Exp conditions	pH*	Target/Rule	Comments
Sol_1	H_2O		30 min, room T	6.8	Soluble fraction	
Sol_2	H_2O		2h, room T	7.1	Soluble fraction	
Exch_1	NH_4 Sulfate	0.05 M	4h, room T	6.8	Exchangeable fraction	Outer-sphere complexes
Exch_2	NH_4 Phosphate Buffer	0.05 M	2h, room T	6.7	Exchangeable fraction	Inner-sphere complexes
Acet	Na Acetic Buffer	1 M	5h, room T	4.7	Carbonates fraction	Dissolution of carbonates
Oxal	NH_4 Oxalate Buffer	0.2 M	2h, room T, dark	3.0	Specifically sorbed fraction	Strongly adsorbed onto amorphous Fe, Al, and Mn oxides
Red_A	Na Dithionite	0.1 M	24h, room T	5.3	Reducing As fraction (strong)	Co-precipitated with Fe-oxides (strong interactions)
Red_B	Ascorbic Acid	0.1 M	24h, room T	2.6	Reducing As fraction (mild)	Co-precipitated with Fe-oxides (weak interactions)
Red_C	NH4 Oxalate	0.1 M	24h, room T	6.8	Reducing As fraction (mild)	Co-precipitated with Fe-oxides (weak interactions)
EDTA	EDTA	0.1 M	24h, room T	4.3	Fe Chelatant	To limit the reprecipitation of As
EDTA/Red_A	EDTA/Dithio	0.1 M	24h, room T	4.8	Reducing As fraction	Co-precipitated with Fe-oxides
EDTA/Red_B	EDTA/Asc	0.1 M	24h, room T	3.5	Reducing As fraction	Co-precipitated with Fe-oxides
EDTA/Red_C	EDTA/Ox	0.1 M	24h, room T	5.2	Reducing As fraction	Co-precipitated with Fe-oxides
NaOCl	NaOCl	5%	24h, room T	9.1	Oxidisable Se fraction	Organic Se fraction
Sulf	Na_2SO_3	1 M	8h, ultrasonic bath	8.6	Oxidisable Se fraction	Elementary Se fraction
NaOH_1	NaOH	1 M	24h, room T	13.5	Alkaline-soluble fraction	OM associated (humic-like) + Clay fraction
NaOH_0.5	NaOH	0.5 M	24h, room T	13.4	Alkaline-soluble fraction	OM associated (humic-like) + Clay fraction
NaOH_0.1	NaOH	0.1 M	24h, room T	11.6	Alkaline-soluble fraction	OM associated (humic-like) + Clay fraction
HNO_3	HNO_3	25%	2h, 70 °C	−0.9	Pyritic fraction	Co-precipitated with pyritic materials

* pH measured in the supernatant after contact time—

Table 2
Description of the sequential extraction scheme.

Code	Reagent	Concentration	Exp. conditions	pH	Target
Sol_2	H_2O		2h/24h, room T	7.1	Soluble fraction
Exch_2	NH_4 Phosphate Buffer	0.05 M	2h/24h, room T	6.7	Exchangeable fraction
Acet	Na Acetic Buffer	1 M	5h/24h, room T	4.7	Carbonates
Oxal	NH_4 Oxalate Buffer	0.2 M	2h/24h, room T, dark	3.0	Amorphous Fe fraction
NaOH_0.1	NaOH	0.1 M	24h, room T	11.6	Alkaline-soluble fraction
HNO_3	HNO_3	25%	2h/24h, 70 °C	−0.9	Pyritic fraction

*: pH measured in the supernatant after the contact time.

detrital materials such as quartz, feldspars, and titanium oxides as described by Bassil et al. (2018) for a similar sedimentary sample (C5-BjC). Calcite and pyrite contents are present at relatively low amounts and the amount of organic matter (5.7%) probably explains the dark color of the sample (Table 3 + Fig. 2).

The studied materials are composed of a brownish clayey matrix (FM for Fine Materials) containing many clasts (CM for Coarse Materials) that are heterogeneous in size and nature, and partially weathered by the organic matter in contact (Fig. 2A). The matrix is also crossed by a dense network of subparallel cracks and coated by a black film attributed to organic matter and infilled by clayey material (Fig. 2B and 2C). The infillings are polyphased (Fig. 2C) and composed of a mixture of cream-white areas attributed to carbonates, and orange/brown areas attributed to iron-oxyhydroxides and are indicative periods of humectation/desiccation suffered by the deposit.

Scanning electronic microscopy mainly focused on the numerous pyrite crystals (bright areas due to the presence of iron) within the clayey matrix (Fig. 3). Three main habitus were identified, as observed by Bassil et al. (2016b), suggesting different mechanisms of formation. Euhedral pyrite (EP), generally formed by direct nucleation and growth in a supersaturated solution, is present locally as micrometric crystals. Large framboidal pyrite (FP) is the main morphology encountered, which results from the

Table 3
Chemical and mineralogical composition of the C5-BjF (this study) and C5-BjC samples (Bassil et al., 2018).

Sample	SiO_2	Al_2O_3	Fe_2O_3	FeO	MnO	MgO	CaO	Na_2O	K_2O	TiO_2	org. C	S Total
	%	%	%	%	%	%	%	%	%	%	%	%
C5-BjF	40.6	30.4	1.8	1.1	< DL	0.3	1.1	0.04	0.07	1.82	5.7	0.57
C5-BjC[a]	39.5	29.2	1.7	ND	< DL	0.3	1.2	0.03	0.06	1.74	8.8	0.61
Sample	**As** mg/kg	**Se** mg/kg	**Pb** mg/kg	**Th** mg/kg	**U** mg/kg	**Σ REE** mg/kg	**Ce** mg/kg	**La** mg/kg	**Ba** mg/kg	**Cs** mg/kg	**Rb** mg/kg	**Sr** mg/kg
C5-BjF	22.4	6.3	56.6	24.3	14.4	812.8	315.5	177.6	19.9	1.4	4.6	20.9
C5-BjC[a]	20.8	2.5	58.9	23.0	47.3	313.4	313.4	178.7	22.2	1.3	4.2	22.4
Sample	**Depth** m		**Calcite** %	**Pyrite** %	**Quartz** %	**Microcline** %	**Anatase** %	**Rutile** %	**Total clay minerals** %			**SSA** $m^2\ g^{-1}$
C5-BjF	67.9		5.0	1.5	10.0	8.0	5.5	–	71			52.2
C5-BjC[a]	68.0		3.0	3.5	3.0	–	8.0	2.0	80			58.6

[a]Bassil et al., 2018.
ND: not determined, < DL: inferior detection limit.

Table 4
Quantifications of the amounts released (in percentage) by single parallel extractions of the sedimentary sample C5-BjF.

Code	% As	SD	% Se	SD	% Fe	SD	% Ca	SD	% Mg	SD	% Al	SD	% Si	SD
Sol_1	**1.3**	0.0	**4.2**	0.1	**0.3**	0.3	**2.0**	0.1	**0.5**	0.0	**0.2**	0.0	**0.2**	0.0
Sol_2	**1.4**	0.4	**5.2**	1.2	**0.2**	0.2	**8.8**	1.8	**0.6**	0.0	**0.3**	0.0	**0.3**	0.1
Exch_1	**0.5**	0.0	**3.7**	0.3	**0.0**	0.0	**71.5**	2.1	**11.6**	0.5	**0.1**	0.0	**0.1**	0.0
Exch_2	**20.6**	1.7	**6.3**	1.2	**0.1**	0.2	**8.4**	0.7	**6.6**	0.7	**0.1**	0.0	**0.1**	0.0
Acet	**15.7**	2.6	**5.5**	0.6	**0.2**	0.1	**98.2**	3.1	**13.7**	3.1	**0.3**	0.0	**0.1**	0.0
Oxal	**34.9**	2.0	**7.4**	1.1	**5.7**	1.0	**0.0**	0.0	**13.4**	0.8	**0.8**	0.1	**0.2**	0.0
Red_A	**20.8**	0.5	**19.6**	0.9	**0.5**	0.0	**77.5**	7.0	**13.4**	1.5	**0.2**	0.0	**0.3**	0.0
Red_B	**29.3**	0.4	**17.7**	1.1	**3.1**	0.2	**48.8**	4.4	**8.9**	1.0	**0.7**	0.0	**0.3**	0.0
Red_C	**26.8**	0.5	**7.8**	0.4	**2.0**	0.2	**0.0**	0.0	**13.1**	1.5	**0.6**	0.0	**0.3**	0.0
EDTA	**28.0**	0.4	**6.6**	0.4	**6.0**	0.5	**100.0**	27.6	**12.4**	1.4	**0.6**	0.0	**0.2**	0.0
EDTA/Red_A	**29.8**	0.7	**19.1**	0.9	**6.1**	0.5	**100.0**	27.5	**12.3**	1.4	**0.7**	0.0	**0.3**	0.0
EDTA/Red_B	**30.6**	0.8	**5.0**	0.4	**5.5**	0.4	**100.0**	29.2	**11.2**	1.3	**0.8**	0.0	**0.4**	0.0
EDTA/Red_C	**31.4**	0.7	**9.8**	0.9	**6.1**	0.5	**18.4**	1.7	**14.3**	1.6	**0.7**	0.0	**0.3**	0.0
NaOCl	**18.2**	4.5	**37.3**	5.5	**0.5**	0.4	**11.7**	1.7	**6.5**	0.7	**0.2**	0.0	**0.2**	0.0
Sulf	**40.0**	8.1	**23.1**	1.3	**1.8**	2.5	**4.7**	0.4	**2.6**	0.3	**0.6**	0.0	**0.1**	0.0
NaOH_1	**38.6**	0.8	**26.0**	1.3	**1.2**	0.4	**3.8**	1.8	**0.0**	0.0	**1.0**	0.1	**0.9**	0.1
NaOH_0.5	**38.9**	0.9	**26.3**	1.2	**1.4**	0.5	**7.3**	3.5	**0.1**	0.1	**1.2**	0.1	**0.6**	0.0
NaOH_0.1	**38.8**	0.6	**26.6**	1.7	**7.2**	2.5	**7.8**	3.7	**5.4**	3.0	**7.7**	0.5	**0.4**	0.0
HNO_3	**57.8**	6.3	**43.8**	1.9	**90.5**	16.4	**83.7**	28.2	**15.4**	5.4	**2.0**	0.1	**0.5**	0.0

transformation of greigite Fe_3S_4 as a precursor, without consensus regarding the involvement of bacterial activity in its formation (Sawlowicz et al., 2005; Wilkin et al., 1996). An intermediate pyrite morphology (IP) is also observed formed due to the progressive cementation of porosity during diagenesis as shown by the overgrowth of microcrystals recrystallized into unfilled framboid and/or euhedral pyrite crystals (Sawlowicz et al., 2005). The spots that appear in bright spots in Fig. 3A are associated with the presence of Fe and S (Fig. 3B and 3D), which confirms the pyritic areas. In other domains, the diffuse distribution of S is partially correlated with the diffuse distribution of calcium (Fig. 3F), indicative of the presence of gypsum (not detected on XRD patterns probably due to low bulk concentration). The Ca-rich areas correspond to the calcite location. Similarly, the diffuse halos of Fe around the pyritic crystals that are uncorrelated with sulfur can be attributed to iron oxyhydroxides.

These observations could be explained by the oxidation of pyrite followed by the precipitation of secondary iron oxyhydroxides according to Equation (1) (Ritsema et al., 1992):

$$4FeS_2 + 15\,O_2 + 14\,H_2O \leftrightarrow 4\,Fe(OH)_3 + 16\,H^+ + 8\,SO_4^{2-} \quad [1]$$

The resulting local acidic medium (vicinity of oxidized pyrites) was neutralized by a reaction between the released protons and the neighboring carbonates, predominantly calcite from the limestone host in the studied case, according to Equation (2) (Ritsema et al., 1992):

$$CaCO_3 + H^+ \leftrightarrow Ca^{2+} + HCO_3^- \quad [2]$$

The released calcium reacts with sulfate to form gypsum according to Equation (3) (Ritsema et al., 1992):

$$CaCO_3 + H^+ + SO_4^{2-} + 2\,H_2O \leftrightarrow CaSO_4\,,2\,H_2O + HCO_3^- \quad [3]$$

The diffuse distribution of Si and Al (Fig. 3C and 3E), which is reverse to that of Fe and S is related to the abundance of clay minerals in the sediment.

Natural pyrite lattices are important hosts of minor and trace elements such as As, Se, Ni, Mo, Co, Cu, Zn, and Pb. The SEM observations and chemical analyses highlighted arsenic "hot spots" in pyrites (Figure S1). These "hot spots" were only observed in the euhedral pyrites, whereas no significant increase of arsenic content was detected in the framboidal pyrites, clay minerals, or carbonates. By contrast, pyrite-associated Se was probably not detected owing to the lower bulk concentration of selenium (6.3 mg/kg) compared to that of arsenic (22.4 mg/kg), rendering the selenium content below the detection limit of the EDX detector. As the euhedral pyritic crystals enriched in arsenic have large diameters, a formation by precipitation in the porosity of the sediment after deposition is assumed in accordance with Bassil et al. (2016b).

3.2. Single parallel extractions (Table 4)

3.2.1. Easily mobilized fractions of arsenic and selenium

Extractions with purified water, a sulfate solution, or a phosphate buffer are expected to only mobilize As or Se oxyanions that are water-soluble or weakly sorbed (outer-sphere complexation for ammonium sulfate and inner-sphere-complexation for phosphate buffer) onto the matrix surface (Javed et al., 2013; Wenzel et al., 2001).

The corresponding fractions (soluble and exchangeable) are expected to represent the immediately available As and Se fractions in the HES groundwater. In the present study, about 5% of selenium is soluble (no significant exchangeable fraction), whereas the easily mobilized As fraction is mainly exchangeable (around 20% against less than 2% for the soluble one).

The speciation of selenium in the soluble fraction mainly consists of SeVI, which is consistent with the species regularly quantified in several wells from the HES. The speciation of arsenic in the soluble fraction is a mixture between AsIII (around 60%) and "non-identified" As, while the arsenic in the specifically-sorbed fraction is exclusively AsV. In the collected groundwater samples from the HES, AsV is predominant, even if high uncertainties related to the quantifications by HPLC-ICP-MS of the soluble As fraction and the low measured concentrations (less than 1 μg/L) were observed.

No significant mobilization of aluminum and iron was observed in these fractions supporting anionic exchange mechanisms. Nevertheless, significant amounts of calcium (and magnesium to a lesser extent) were quantified in the soluble fraction (nearly 2%), the non-specifically sorbed one (around 70%), and the specifically sorbed one (around 8%).

The behaviors of arsenic and selenium do not seem to be linked to the dissolution of carbonates, although it is not excluded that calcite is an effective scavenger of trace elements including arsenic and selenium (Costagliola et al., 2013; Renard et al., 2015; Rios-Valenciana et al., 2020).

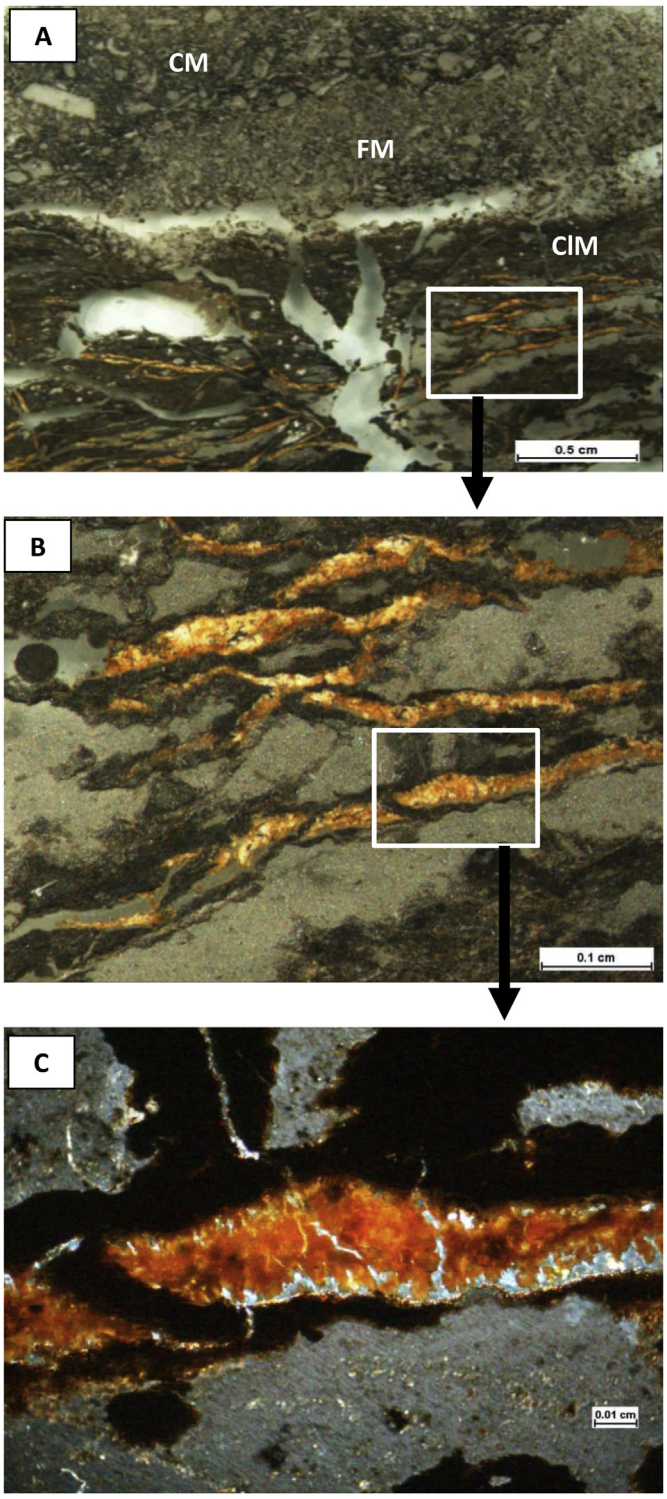

Fig. 2. Petrographic observations on polished thin sections (A) of the sedimentary sample C5-BjF; (B) and (C) are detailed view of regions of interest. The infilling material is composed of mixture of carbonates (white) and iron oxyhydroxides (ochreous). CM: coarse material, FM: fine material, ClM: clay matrix.

3.2.2. Fraction of arsenic and selenium associated with carbonates

Selenium released concomitantly with the dissolution of carbonates (calcite, and dolomite to a lesser extent) is comparable to the soluble Se fraction observed in the previous paragraph, suggesting that no detectable selenium is trapped in the carbonated matrix. This observation is consistent with the results of Bassil et al. (2016a) performed with a similar sample (Table 3), and supports that the origin of selenium in the Dogger aquifer is related to the clayey karst infilling materials and not to the limestone host.

Arsenic fraction associated with carbonates (about 15%) seems to be included in the exchangeable As fraction (about 20%). This observation suggests that no detectable arsenic is present in the carbonates and also tends to show that acetate buffer through its carboxylate group favors the release of specifically sorbed arsenic, less efficiently than phosphate ions, or as efficiently with a later reprecipitation or re-complexation of arsenic.

3.2.3. Co-precipitated fraction of arsenic (and selenium) with amorphous Fe oxyhydroxides

Significant amounts of iron (II and III) were quantified in the studied sample, but only pyrite was detected by XRD measurements (Table 3). These observations could be explained by the presence of amorphous or poorly crystallized FeIII oxyhydroxides identified by SEM/EDX but hardly detected by XRD, or by a low occurrence of crystallized Fe-containing minerals.

In parallel, petrographic investigations show the presence of pyritic crystals altered into gypsum and iron-bearing minerals such as poorly crystallized oxides or oxyhydroxides (Fig. 3). After weathering, arsenic initially associated with pyrite could have been coprecipitated with iron minerals or possibly reprecipitated as scorodite in the immediate vicinity (Kim et al., 2015).

Ammonium oxalate buffer was used to enhance the dissolution of poorly crystallized iron-bearing minerals (Panias et al., 1996) according to the following sequence: (1) adsorption of the carboxylate group onto the surface, (2) non-reductive dissolution through direct desorption, and then (3) reductive dissolution of iron. During the reduction phase, visible light mediates electron transfer on the surface of ferric-oxalate complexes, providing a supplementary pathway for the dissolution of oxides. Dark conditions were thus preferred to limit an over-estimation of released arsenic.

Arsenic release associated with poorly crystallized iron oxyhydroxides is significantly higher (nearly 35%) than the amounts mobilized with the previous single extractants, supporting the assumption that after pyrites weathering, the arsenic initially present in their structure could have coprecipitated with secondary iron minerals or reprecipitated as scorodite ($FeAsO_4$, $2H_2O$) in the immediate vicinity (Kim et al., 2015). Iron release corresponds only to around 5%, confirming the relatively high proportion of arsenic associated with secondary iron oxides and oxyhydroxides.

The speciation of released arsenic with the oxalate buffer is mainly AsV as observed with the exchangeable fraction, consistent with the speciation generally observed for scorodite or coprecipitated iron phases (Kim et al., 2015).

Even if all the calcium released has been reprecipitated as calcium oxalate, the presence of soluble magnesium tends to show that carbonates (calcite and dolomite) were also dissolved concomitantly to amorphous iron minerals. Despite the low pH (Table 1), no significant amount of soluble aluminum was quantified in the extraction solution suggesting the absence of amorphous Al-bearing minerals.

Selenium release slightly increases (around 7.5%) compared to the soluble Se fraction (around 5%) and could be attributed to a specifically sorbed Se fraction onto iron-bearing minerals (Börsig et al., 2017; Fernández-Martínez and Charlet, 2009).

3.2.4. Reducible fraction of arsenic (and selenium)

Reducing agents of different strengths (sodium dithionite (RedA), ascorbic acid (RedB), and ammonium oxalate (RedC)) were

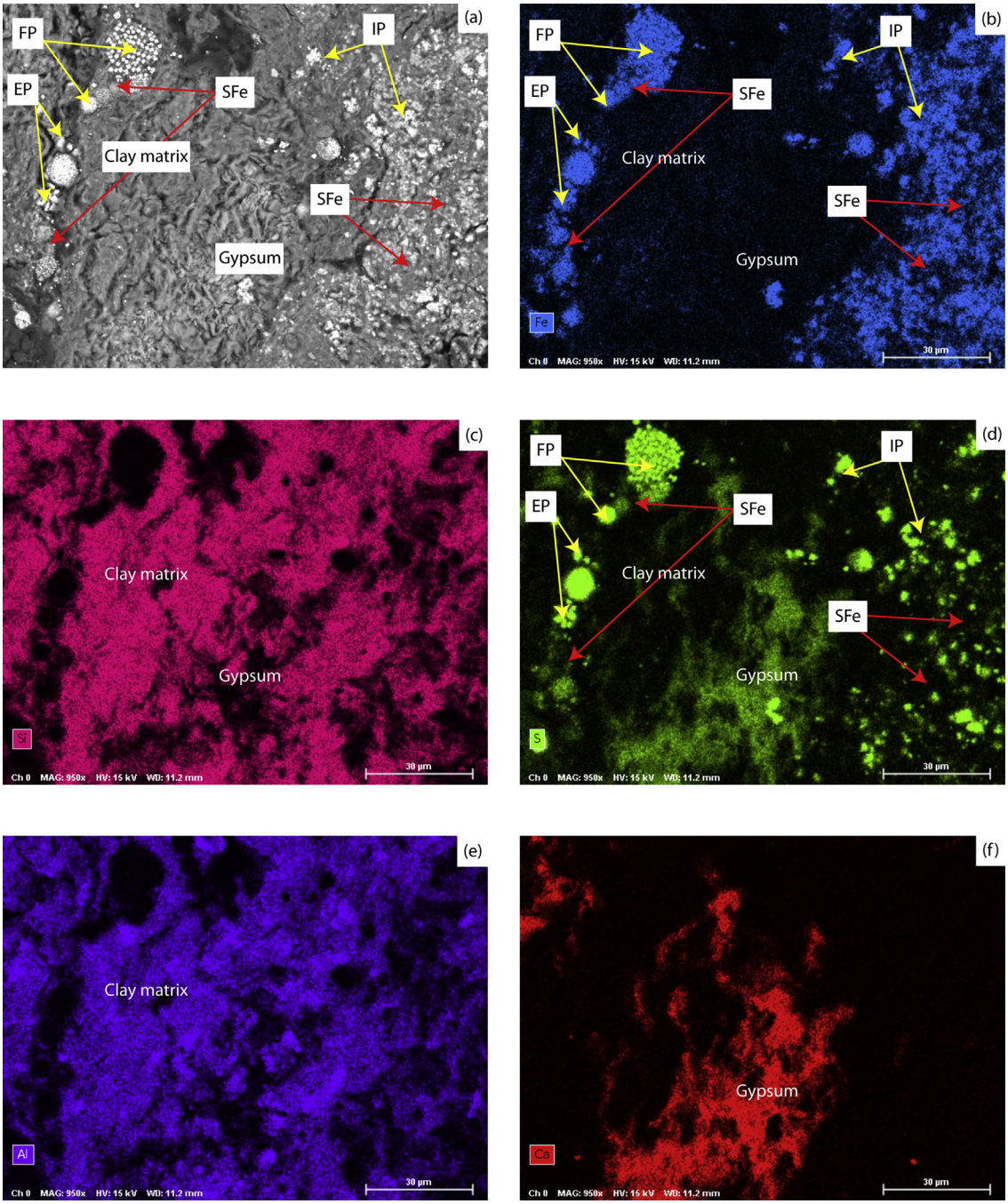

Fig. 3. Scanning electron micrograph (a) of selected area of pyritized clay matrix of the C5-BjF sample, elemental maps for (b) Fe, (c) Si, (d) S, (e) Al, and (f) Ca. Pyrites are identified by the presence of Fe and S; Clay minerals are identified by the presence of Si and Al. Gypsum is identified by presence of Ca and S. FP: framboidal pyrites; EP: euhedral pyrites; IP: intermediate morphology pyrite.

tested to favor the dissolution of iron-bearing minerals and enhance the solubility of arsenic through reduction of AsV into AsIII. Combinations with a strong chelating agent (EDTA) were also performed to limit the interactions between arsenic oxyanions and the ferrous soluble species or the newly formed iron oxide phases (Kim et al., 2015). None of the extractants (EDTA alone, reducing agent alone, or a mix) was more efficient than the oxalate buffer to mobilize arsenic from the studied sample, despite a higher mobilization of iron in the presence of EDTA (6.1% against 4.6% with the oxalate buffer). Even if relatively well-crystallized iron oxides could be targeted in the present fraction, reprecipitation and recomplexation of arsenic onto the surfaces is expected and EDTA seems to be the limiting factor.

No mobilization of selenium was expected with reducing agents, but sodium dithionite generates an important release of selenium (nearly 20%). This observation is explained by the inherent instability of dithionite that can produce powerful oxidizing radicals for selenium compounds (Geoffroy and Demopoulos, 2009), or the formation of colloidal elemental selenium that could pass through filtration membranes. The important release of selenium with ascorbic acid (about 18%) tends to favor this second assumption.

No significant amount of soluble aluminum was quantified,

whereas all the initial calcium was mobilized in the presence of EDTA. Reprecipitation of calcium oxalate was also observed by XRD.

3.2.5. Oxidisable fraction of selenium (and arsenic)

Sodium hypochlorite (NaOCl) is an efficient extractant of the organic matter however, no significant fraction of arsenic was extracted using this reagent (comparable release as the exchangeable fraction). The amount of Se extracted by NaOCl, on the other hand, was significant (about 10% estimated by difference).

Surprisingly, an important amount of arsenic (around 40%) was mobilized with the oxidizing agent sodium sulfite. This reagent associated with light and iron can generate the photooxidation of AsIII into AsV, but this reaction is highly sensitive to the initial amount of sulfite and the pH conditions (Xu et al., 2016). In other conditions (Zakharova et al., 2015), sodium sulfite can also be used as a photo-reductive reagent.

The present reagent targeted the elemental selenium initially present in the sediment and generated unexpected reactions with arsenic, however further investigations onto the speciation of the released arsenic are necessary to better understand the processes involved in the present case.

3.2.6. Alkaline-soluble fraction of arsenic and selenium

The studied karst infillings contain relatively high amounts of organic matter (Table 3), degradation products of vascular plants that have been transported from the surface into karst cavities (Bassil et al., 2016a). Associations between the humic-like organic matter and arsenic and selenium were targeted using different concentrations of sodium hydroxide (NaOH 0.1, 0.5, and 1 M).

A significant alkaline-soluble fraction for both arsenic and selenium is observed, but the concentration of sodium hydroxide has no influence on the mobilization of arsenic (around 40%) and selenium (around 25%). Concomitantly, the lowest basic conditions clearly enhance the mobilization of aluminum (about 8%) and iron (about 10%), whereas the amount of organic C released (around 10%) tends to increase with increasing basic conditions. Similar results were observed with different proportions (85% of Se released and 21% of organic C and 2% Fe released) by Bassil et al. (2016a), who have attributed the partial mobilization of iron in alkaline conditions to the presence of complexed species. No significant release of Si was observed, suggesting the absence of dissolution of the clay minerals as confirmed by the corresponding X-ray diffractograms (Fig. 1).

The As fraction associated with the organic matter is thus estimated at around 5%, with a speciation corresponding to a mix between AsIII (around 23%) and AsV (around 77%), whereas the Se alkaline-soluble fraction tends to reach about 10%.

3.2.7. Fraction of arsenic and selenium associated with pyrite

As expected by the mineralogical and petrographic investigations, a significant As pyritic fraction was extracted using hot nitric acid. In addition, a significant Se fraction was also observed at this step.

The pyritic fraction can be thus estimated by subtraction, at around 15% and 20%, for arsenic and selenium, respectively. Under hot nitric treatment, the mobilization of the studied elements is associated with the mobilization of almost all iron - and calcium - content of the sedimentary sample, confirming the low selectivity of this reagent (Kulp and Pratt, 2004), thus mobilizing the arsenic "trapped" with all the iron-bearing minerals, both primary (sulfides) and secondary (oxides and oxyhydroxides).

3.2.8. Synthesis of single parallel extractions

In addition to the significant soluble Se fraction (about 5%), consistent with the presence of selenium species quantified in different wells drilled into the Dogger aquifer of the HES, this element seems to be associated with pyrite and, to a lesser extent, to their alteration products and organic matter. Neither significant association with the carbonates, nor the presence of elemental selenium, was highlighted by the present series of single parallel extractions.

Concerning arsenic, a very low soluble fraction was observed compared to its relatively important exchangeable fraction (about 20%). As for selenium and consistently with the microscopic investigations, the distribution of arsenic seems to be mainly limited to the pyritic crystals and the secondary iron-bearing minerals present in the sedimentary clayey matrix.

Statistical analyses (Figs. S2 and S3)support the present observations by highlighting the high correlation coefficients between the released amounts of arsenic and iron ($r = 0.78$), selenium and iron ($r = 0.89$), and arsenic and selenium ($r = 0.87$). In parallel, no significant positive correlation was shown between the three previous elements and calcium, aluminum, or pH conditions.

3.3. Sequential chemical extraction

To refine the major points brought to light by the series of parallel extractions experiments, a simplified sequential extraction scheme (Table 2) was defined using both the results of paragraph 3.2. and the characterization of the sedimentary matrix (paragraph 3.1.). Two contact times– except for NaOH – were also tested to better understand the effect of contact time on the mechanisms involved in the release of the two elements.

3.3.1. Behavior of arsenic

In accordance with the parallel extractions, the easily mobilized fraction of arsenic is mainly exchangeable (about 13%) with a low soluble fraction (less than 2%) (Fig. 4A). A longer contact time has no impact on the soluble fraction, but significantly increases the exchangeable one (from 13.3% to 22.2%) (Fig. 4B). This point could be of high concern in-situ, leading to an important arsenic mobilization under slight changes in the ionic composition of the groundwater induced by pumping or climatic changes (Smedley and Kinniburgh, 2002).

A low but significant As fraction associated with carbonates (about 8.5%) was identified by the sequential scheme, contrary to the parallel one, and tends to decrease with a longer contact time (Fig. 4). It is assumed that part of this fraction was extracted in the previous steps, the dissolution of carbonates being favored by longer contact times. But, in the present case, the amounts of mobilized calcium totally invalidate this assumption and tend to support that the arsenic associated with calcite may be released by other mechanisms, such as the desorption of weakly-sorbed fraction (Rios-Valenciana et al., 2020). It is to note that all the calcium has been extracted at this step, as confirmed by the chemical and mineralogical analyses (Figs. 1 and 4).

The As fraction associated with alteration products of the pyritic materials, described through SEM-EDX pictures as diffuse and poorly crystallized iron oxides corresponds to about 13% of the total arsenic initially present in the matrix, consistently with the estimation performed with the parallel extractions. The amount of mobilized iron is refined to 7.4% and slightly increases for a longer contact time to 8.3%. The concomitant decrease of the As release is attributed, as for the fraction associated with the carbonates, to a partial extraction of this fourth fraction during the longer contact time with phosphate buffer, whose pH and complexing properties cannot prevent iron reprecipitation.

The As fraction associated with organic matter is relatively low (less than 5%) in accordance with the parallel extractions, whereas the pyritic fraction is the most important (about 35%) as expected

Fig. 4. Released amounts (in percentage) of arsenic, selenium, iron, calcium, aluminum, and silicon for a contact time of 2h (a) and 24h (b) by the sequential extraction scheme. (For interpretation of the references to color in this figure legend, the reader is referred to the Web version of this article.)

by the elemental spatial distribution (Figure S1). This amount was highly underestimated by parallel extractions whereas all the iron was mobilized. This amount is not dependent on the contact time and tends to show that about 80% of the iron present in the matrix was initially pyritic.

About 25% of arsenic was finally refractory to the present sequential extraction scheme, assumingly as well-crystallized As oxides, sulfides, or coprecipitated with the 7.5% of refractory iron (Javed et al., 2013).

3.3.2. *Behaviour of selenium*

In accordance with the parallel extractions and the presence of selenium in the HES groundwater, the easily mobilized fraction of selenium is mainly soluble (about 5%) with a low exchangeable fraction (less than 1%). A longer contact time seems to slightly increase the soluble fraction at the expense of the exchangeable one. This point could explain the progressive increase of the selenium concentrations measured in the HES wells poorly connected to the other wells, and thus containing stagnant waters (not published).

No significant Se fraction associated with the carbonates was quantified as estimated by parallel extractions experiments, supporting that selenium was not originated from the limestone host of the Dogger aquifer. The fraction associated with secondary iron-bearing minerals and probably specifically sorbed onto their surface is low (about 2%), whereas the Se fraction associated with organic matter is relatively important (nearly 18%). The contact time has no significant influence on the amounts released.

As observed for arsenic, the Se pyritic fraction was highly underestimated by parallel extractions and reached 39% of the initial selenium in the matrix. This amount suggests the presence of pyrite-associated selenium that was not observed by SEM-EDX.

The important refractory Se fraction (around 37%) is attributed to the absence of adapted reagents (mainly oxidizing reagents targeting elemental and organic selenium) in the sequential scheme.

3.3.3. *Synthesis of sequential extractions scheme*

The combination of petrographic and mineralogical investigations with the sequential extractions experiments suggests that pyritic minerals are the main initial hosts of arsenic and selenium in the clayey karst infillings present in the Dogger aquifer. The alteration of these primary minerals had assumingly favored

the partial mobilization of selenium and arsenic followed by reprecipitation and sorption processes with other constituents of the matrix or with secondary minerals. At this step, the pathways of selenium and arsenic tend to diverge: arsenic is mainly associated with secondary iron oxides, as already mentioned by Javed et al. (2013), in part with calcite, and barely with the organic matter, whereas selenium is mainly associated with the organic matter, as described by Gustafsson and Johnsson (1994) and Li et al. (2017), barely with the secondary iron oxides, and not significantly with the limestone host.

Strong significant positive correlations (Figure S2) are additionally observed (and enhanced) between the released amounts of arsenic and iron ($r = 0.94$) and between those of selenium and iron ($r = 0.90$). Sequential extractions and longer contact times tend to decrease the correlation between arsenic and selenium ($r = 0.75$) compared to single parallel experiments ($r = 0.87$), supporting their divergence. Concomitantly, the behavior of aluminum seems to follow the release of selenium, iron, and arsenic. This correlation tends to be reinforced with longer contact times suggesting that more complex release mechanisms could be involved.

In parallel, negative correlations are observed between the released amounts of arsenic and the pH conditions ($r = -0.80$), but not for selenium ($r = -0.35$). Leaching studies as a function of pH were performed for a better understanding of the mechanisms induced in the behavior of these elements.

3.4. Leaching studies as a function of pH

As previously observed by (Bassil et al., 2018; Tabelin et al., 2012), arsenic and selenium release behaviors are strongly dependent on acid-base conditions (Fig. 5). In very acidic conditions (below pH 2), the releases of As (Fig. 5A) and Se (Fig. 5B) sharply increase with the pH decrease. This concomitant and consistent release behavior is attributed to the partial dissolution of pyrite, previously identified as the main host for As using the chemical extractions and SEM-EDX.

In basic conditions (above pH 8), the As and Se releases sharply increase with the pH to reach a maximum at around pH 12 (Fig. 6). These releases are again concomitant for both elements. The release patterns of Fe and Al are similar, but occur at slightly higher pH (about one pH unit) than for As and Se. The release pattern of TOC also occurs in more alkaline conditions (about one additional pH unit).

As highlighted by the statistical results, Fe and Al behaviors tend to be closely correlated in basic pH conditions, as if they were complexed to the same species, probably with the humic-like organic matter, as already described for soils (Jansen et al., 2011; Wagai et al., 2013). Even if significant correlations are observed with TOC, the mobilization of the sedimentary organic matter seems to be indirectly associated with the release of other elements.

These observations converge to the ideas that (1) the alkaline-soluble fractions are only ruled by desorption processes and not by dissolution, contrary to the mobilizations observed in acidic pH conditions, and (2) the observed desorption processes are associated with the change in the surface charge.

If the behaviors of arsenic and selenium are strictly concomitant below pH 2 and above pH 8, they strongly diverge between pH 2 and 8. The soluble selenium is thus nearly constant at around 5% in this pH range, when the mobilized arsenic decreases from about 10% at pH 2 to less than 1% at circumneutral pH.

It is interesting to observe that the amounts of arsenic and selenium released after 1 week of contact time in purified water are consistent with the amounts extracted after 2h of contact time. The soluble fraction thus consists of an easily released fraction of the studied elements. In the same way, the released amounts of arsenic (around 25%) and selenium (around 35%) in the basic plateau correspond to the 'alkaline-soluble' fractions previously quantified for a contact time of 24 h, and support rapid mechanisms.

In parallel, all the quantities of selenium released by selective chemical extractions are consistent with the leaching experiments, and thus show that selenium mobilization is mainly governed by the acid-base conditions of the medium in contact. On the contrary, the presence of complexing agents such as the ones used in the extractions experiments (phosphate, acetate, and oxalate anions), tends to favor and control the mobilization of arsenic species in the system by preventing them from reprecipitation or resorption onto surfaces.

Finally, as assumed by the previous experiments and statistical studies, Ca and Mg behaviors are highly related but not directly correlated to the behaviors of arsenic and selenium.

4. Conclusion

The Upper Cretaceous clayey materials that fill partly the karst cavities formed into the Bajocian limestone of the Dogger aquifer, are important geogenic sources of arsenic and selenium traces found in regional groundwaters. Correlating the origin, the

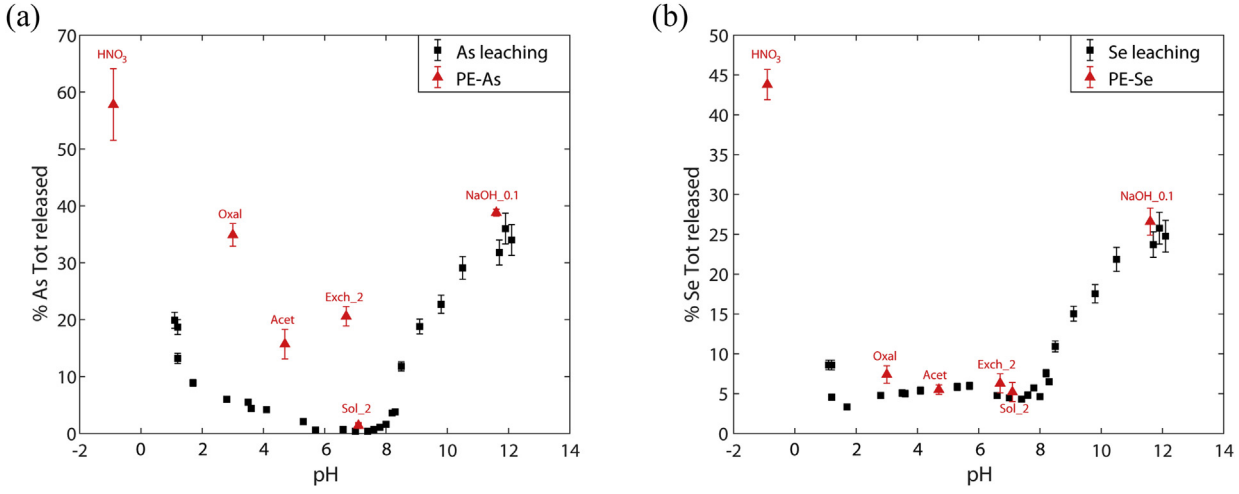

Fig. 5. Released amounts (in percentage) of (a) arsenic and (b) selenium as a function of pH (contact time of 1 week). PE: Parallel extraction results.

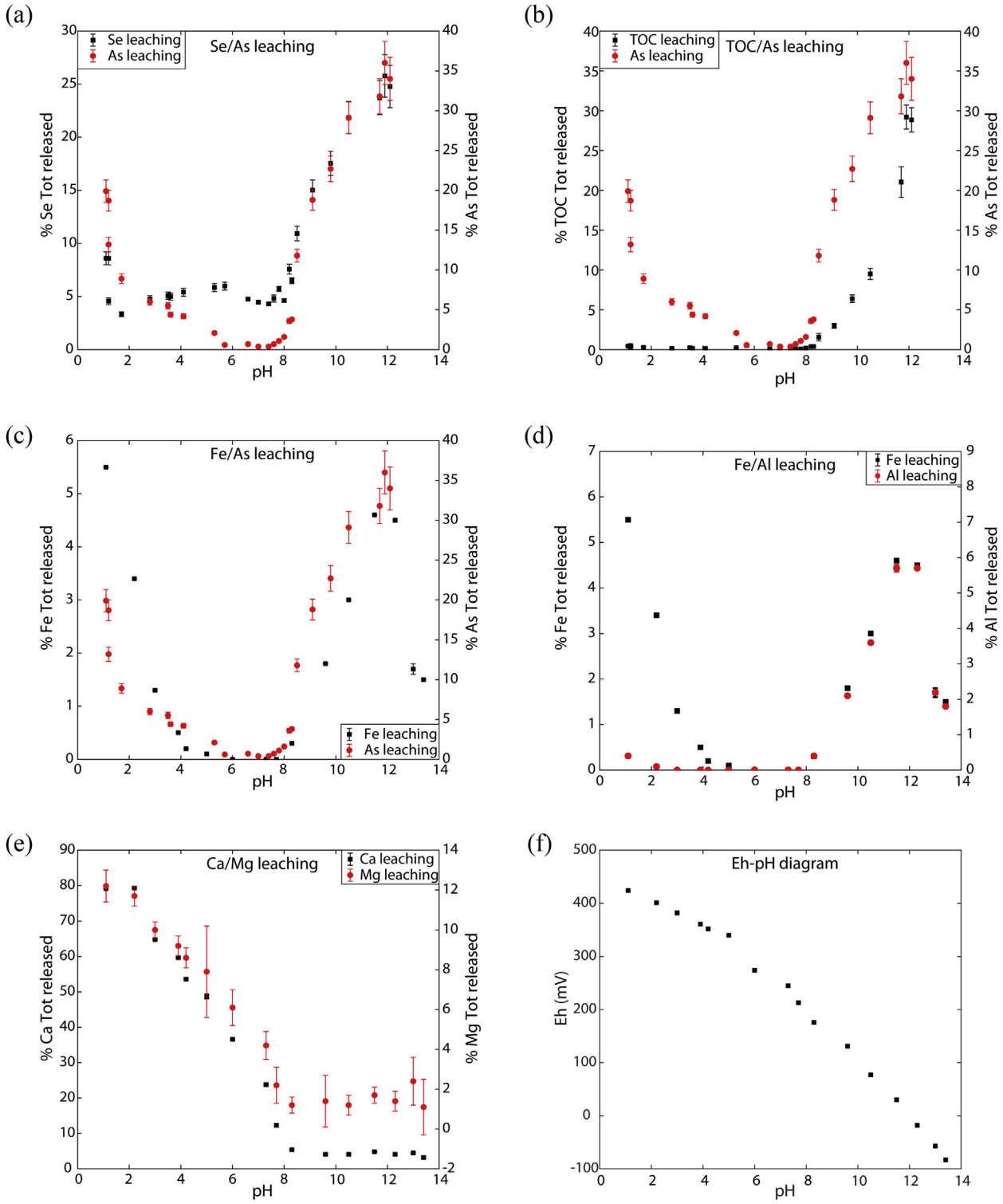

Fig. 6. Released amounts (in percentage) of (a) arsenic/selenium; (b) total organic carbon/arsenic; (c) iron/arsenic; (d) iron/aluminum; (e) calcium/magnesium; (f) Eh as a function of pH (contact time of 1 week).

distribution, and the release mechanisms of these two micro-pollutants was expected to better understand their behavior into a fractured carbonate aquifer.

The combination of petrographical investigations with chemical extractions, leaching experiments, and statistical analysis highlighted the pyritic origin of both elements. Arsenic "hot spots" were observed within euhedral pyritic crystals and into the surrounding halo of secondary iron-bearing minerals resulting from their oxidative alteration. Even though selenium-associated pyrite was not directly observed by SEM-EDX images, the chemical extractions showed the existence of an important selenium pyritic fraction. Nevertheless, the affinity of selenium for secondary iron-bearing

minerals is lower than that of arsenic, and alteration of pyritic minerals has favored associations of selenium species with the humic-like sedimentary organic matter.

These divergences of associations have no impact on the mobilization of both elements in very acidic conditions, controlled by the partial dissolution of pyritic materials, and in alkaline conditions (above pH 8), ruled by desorption processes and especially by the reactivity of the involved surfaces. The main divergences in both elements' behaviors are observed between pH 2 and 8, leading to a soluble fraction of about 5% for selenium, and a very low soluble fraction for arsenic (lower than 2%) in the pH range [6.9 - 7.9] measured in the groundwater of the Dogger aquifer.

The main components of the limestone aquifer (calcite and dolomite to a lesser extent) are not directly associated with the mobilization of the studied elements but, in such context, $Ca-Mg-CO_2-H_2O$ equilibrium highly constrains the pH conditions of the groundwater close to neutrality. The leaching experiments also contradicted their apparent correlation with the mobilization of iron, aluminum, and TOC, highlighted by previous studies and the present statistical analyses and extractions protocols.

Except in very acidic conditions, the behavior of selenium seems to be only ruled by surface complexation equilibria, and therefore by the pH conditions of the medium in contact. Although the pH of the groundwater is buffered by the carbonate aquifer, local acidic conditions may occur at the vicinity of pyrites due to their oxidation. This process can be enhanced by water pumping from wells of the aquifer, which induces more oxidizing conditions.

The mobilization of arsenic is more complex: although the soluble fraction in percentage is very low in the pH range of the HES groundwater, the amounts of arsenic released are in the same order of magnitude as those of selenium. In parallel, even if arsenic mobilization is also highly pH-dependent and mainly ruled by sorption processes, the impact of complexing agents such as phosphate or small organic acids (acetate, oxalate) that can be naturally present in the groundwater is important (and roughly corresponds to about 20%). According to the present results, arsenic should be detected in the water sampling campaigns in the Dogger aquifer, however this is not the case. Further investigations will thus be necessary to bring to light the impact of natural chelating agents on the stability of the surface complexes formed with arsenic and selenium species in the pH range imposed by the carbonates of the aquifer.

Credit roles

Conceptualization, Laurent Caner, Aude Naveau, and Rana Mhanan. Methodology, Aude Naveau, Claude Fontaine, Maite Bueno, and Rana Mhanna. Software, Aude Naveau, Claude Fontaine, and Rana Mhanna. Validation, Aude Naveau, Laurent Caner, and Joseph Bassil. Formal analysis, Aude Naveau, Laurent Caner, and Rana Mhanna. Investigation, Rana Mhanna, Fatima Ismail, Majd Shmeit. Resources, Aude Naveau, Gilles Porel and Claude Fontaine. Data curation, Aude Naveau and Rana Mhanna. Writing – original draft, Preparation Rana Mhanna and Aude Naveau. Writing – review & editing, All authors. Visualization, Aude Naveau, Laurent Caner, Rana Mhanna, and Claude Fontaine. Supervision, Laurent Caner and Aude Naveau. Project administration, Laurent Caner. Funding acquisition, Aude Naveau.

Declaration of competing interest

The authors declare that they have no known competing financial interests or personal relationships that could have appeared to influence the work reported in this paper.

Acknowledgments

We acknowledge the financial support from the European Union, the 'Région Nouvelle Aquitaine' and the 'Agence de l'Eau Loire-Bretagne'. We also acknowledge C. Boissard and J. Rousseau for their technical support to the petrographic investigations.

Appendix A. Supplementary data

Supplementary data to this article can be found online at https://doi.org/10.1016/j.chemosphere.2021.129935.

References

Audouin, O., Bodin, J., Porel, G., Bourbiaux, B., 2008. Flowpath structure in a limestone aquifer: multi-borehole logging investigations at the hydrogeological experimental site of Poitiers, France. Hydrogeol. J. 16, 939–950. https://doi.org/10.1007/s10040-008-0275-4.

Bassil, J., Naveau, A., Bueno, M., Di Tullo, P., Grasset, L., Kazpard, V., Razack, M., 2016a. Determination of the distribution and speciation of selenium in an argillaceous sample using chemical extractions and post-extractions analyses: application to the hydrogeological experimental site of Poitiers. Environ. Sci. Pollut. Res. 23, 9598–9613. https://doi.org/10.1007/s11356-016-6113-7.

Bassil, J., Naveau, A., Fontaine, C., Grasset, L., Bodin, J., Porel, G., Razack, M., Kazpard, V., Popescu, S.-M., 2016b. Investigation of the nature and origin of the geological matrices rich in selenium within the Hydrogeological Experimental Site of Poitiers, France. Compt. Rendus Geosci. 348, 598–608. https://doi.org/10.1016/j.crte.2016.08.004.

Bassil, J., Naveau, A., Bueno, M., Razack, M., Kazpard, V., 2018. Leaching behavior of selenium from the karst infillings of the hydrogeological experimental site of Poitiers. Chem. Geol. 483, 141–150. https://doi.org/10.1016/j.chemgeo.2018.02.032.

Börsig, N., Scheinost, A.C., Shaw, S., Schild, D., Neumann, T., 2017. Uptake mechanisms of selenium oxyanions during the ferrihydrite-hematite recrystallization. Geochem. Cosmochim. Acta 206, 236–253. https://doi.org/10.1016/j.gca.2017.03.004.

Chen, C.J., Chen, C.W., Wu, M.M., Kuo, T.L., 1992. Cancer potential in liver, lung, bladder and kidney due to ingested inorganic arsenic in drinking water. Br. J. Canc. 66 (5), 888–892.

Chung, F.H., 1975. Quantitative interpretation of X-ray diffraction patterns. III. Simultaneous determination of a set of reference intensities. J. Appl. Crystallogr. 8, 17.

Costagliola, P., Bardelli, F., Benvenuti, M., Di Benedetto, F., Lattanzi, P., Romanelli, M., Paolieri, M., Rimondi, V., Vaggelli, G., 2013. Arsenic-bearing calcite in natural travertines: evidence from sequential extraction, μXAS, and μXRF. Environ. Sci. Technol. 47, 6231–6238. https://doi.org/10.1021/es304953a.

European Union, 1998. Council directive 98/83/EC on the quality of water intended for human consumption. Official Journal of the European Communities 32–54. L 330/32.

Fernández-Martínez, A., Charlet, L., 2009. Selenium environmental cycling and bioavailability: a structural chemist point of view. Rev. Environ. Sci. Biotechnol. 8, 81–110. https://doi.org/10.1007/s11157-009-9145-3.

Geoffroy, N., Demopoulos, G.P., 2009. Reductive precipitation of elemental selenium from selenious acidic solutions using sodium dithionite. Ind. Eng. Chem. Res. 48, 10240–10246. https://doi.org/10.1021/ie9008502.

Gustafsson, J.P., Johnsson, L., 1994. The association between selenium and humic substances in forested ecosystems—laboratory evidence. Appl. Organomet. Chem. 8, 141–147. https://doi.org/10.1002/aoc.590080209.

Hillier, S., 2000. – Accurate quantitative analysis of clay and other minerals in sandstones by XRD comparison of a Rietveld and a reference intensity ratio (RIR) method and the importance of sample preparation. Clay Miner. 35, 291–302.

Jansen, B., Tonneijck, F.H., Verstraten, J.M., 2011. Selective extraction methods for aluminium, iron and organic carbon from montane volcanic ash soils. Pedosphere 21, 549–565. https://doi.org/10.1016/S1002-0160(11)60157-4.

Javed, M.B., Kachanoski, G., Siddique, T., 2013. A modified sequential extraction method for arsenic fractionation in sediments. Anal. Chim. Acta 787, 102–110. https://doi.org/10.1016/j.aca.2013.05.050.

Javed, M.B., Kachanoski, G., Siddique, T., 2014. Arsenic fractionation and mineralogical characterization of sediments in the Cold Lake area of Alberta, Canada. Sci. Total Environ. 500– 501, 181–190. https://doi.org/10.1016/j.scitotenv.2014.08.083.

Jegadeesan, G., Al-Abed, S.R., Pinto, P., 2008. Influence of trace metal distribution on its leachability from coal fly ash. Fuel 87, 1887–1893. https://doi.org/10.1016/j.fuel.2007.12.007.

Kim, E.J., Jeon, E.-K., Baek, K., 2016. Role of reducing agent in extraction of arsenic and heavy metals from soils by use of EDTA. Chemosphere 152, 274–283. https://doi.org/10.1016/j.chemosphere.2016.03.005.

Kim, E.J., Lee, J.-C., Baek, K., 2015. Abiotic reductive extraction of arsenic from contaminated soils enhanced by complexation: arsenic extraction by reducing

agents and combination of reducing and chelating agents. J. Hazard Mater. 283, 454–461. https://doi.org/10.1016/j.jhazmat.2014.09.055.
Kim, E.J., Yoo, J.-C., Baek, K., 2014. Arsenic speciation and bioaccessibility in arsenic-contaminated soils: sequential extraction and mineralogical investigation. Environ. Pollut. 186, 29–35. https://doi.org/10.1016/j.envpol.2013.11.032.
Kulp, T.R., Pratt, L.M., 2004. Speciation and weathering of selenium in upper cretaceous chalk and shale from South Dakota and Wyoming, USA. Geochem. Cosmochim. Acta 68, 3687–3701. https://doi.org/10.1016/j.gca.2004.03.008.
Le Coz, M., Bodin, J., Renard, P., 2017. On the use of multiple-point statistics to improve groundwater flow modeling in karst aquifers: a case study from the Hydrogeological Experimental Site of Poitiers. France. J. Hydrol. 545, 109–119. https://doi.org/10.1016/j.jhydrol.2016.12.010.
Li, Z., Liang, D., Peng, Q., Cui, Z., Huang, J., Lin, Z., 2017. Interaction between selenium and soil organic matter and its impact on soil selenium bioavailability: a review. Geoderma 295, 69–79. https://doi.org/10.1016/j.geoderma.2017.02.019.
Mari, J.L., Porel, G., Delay, F., 2020. Contribution of full wave acoustic logging to the detection and prediction of karstic bodies. Water 12, 948. https://doi.org/10.3390/w12040948.
Martens, D.A., Suarez, D.L., 1997. Selenium speciation of soil/sediment determined with sequential extractions and hydride generation atomic absorption spectrophotometry. Environ. Sci. Technol. 31, 133–139. https://doi.org/10.1021/es960214+.
Matamoros-Veloza, A., Newton, R.J., Benning, L.G., 2011. What controls selenium release during shale weathering? Appl. Geochem. 26, S222–S226. https://doi.org/10.1016/j.apgeochem.2011.03.109.
Nakamaru, Y.M., Altansud, J., 2014. Speciation and bioavailability of selenium and antimony in non-flooded and wetland soils: a review. Chemosphere 111, 366–371.
Panias, D., Taxiarchou, M., Paspaliaris, I., Kontopoulos, A., 1996. Mechanisms of dissolution of iron oxides in aqueous oxalic acid solutions. Hydrometallurgy 42, 257–265. https://doi.org/10.1016/0304-386X(95)00104-O.
Raessler, M., 2018. The arsenic contamination of drinking and groundwaters in Bangladesh: featuring biogeochemical aspects and implications on public health. Arch. Environ. Contam. Toxicol. 75, 1–7. https://doi.org/10.1007/s00244-018-0511-4.
Renard, F., Putnis, C.V., Montes-Hernandez, G., Ruiz-Agudo, E., Hovelmann, J., Sarret, G., 2015. Interactions of arsenic with calcite surfaces revealed by in situ nanoscale imaging. Geochem. Cosmochim. Acta 159, 61–79. https://doi.org/10.1016/j.gca.2015.03.025.
Rios-Valenciana, E.E., Briones-Gallardo, R., Chazaro-Ruiz, L.F., Lopez-Lozano, N.E., Sierra-Alvarez, R., Celis, L.B., 2020. Dissolution and final fate of arsenic associated with gypsum, calcite, and ferrihydrite: influence of microbial reduction of As(V), sulfate, and Fe(III). Chemosphere 239, 124823. https://doi.org/10.1016/j.chemosphere.2019.124823.
Ritsema, C.J., Groenenberg, J.E., Bisdom, E.B.A., 1992. The transformation of potential into actual acid sulphate soils studied in column experiments. Geoderma 55, 259–271. https://doi.org/10.1016/0016-7061(92)90087-N.
Rosen, B.P., Liu, Z., 2009. Transport pathways for arsenic and selenium: a minireview. Environ. Int. 35, 512–515. https://doi.org/10.1016/j.envint.2008.07.023.
Sawlowicz, Z., Łatkiewicz, A., Stefaniak, E., 2005. Two-dimensional natural pyrite crystals and their formation. Mineral. Mag. 69, 455–461. https://doi.org/10.1180/0026461056940263.
Smedley, P.L., Kinniburgh, D.G., 2002. A review of the source, behaviour and distribution of arsenic in natural waters. Appl. Geochem. 17, 517–568. https://doi.org/10.1016/S0883-2927(02)00018-5.
Su, T., Wang, J., 2011. Modeling batch leaching behavior of arsenic and selenium from bituminous coal fly ashes. Chemosphere 85, 1368–1374. https://doi.org/10.1016/j.chemosphere.2011.08.002.
Tabelin, C.B., Igarashi, T., Yoneda, T., 2012. Mobilization and speciation of arsenic from hydrothermally altered rock containing calcite and pyrite under anoxic conditions. Appl. Geochem. 27, 2300–2314. https://doi.org/10.1016/j.apgeochem.2012.07.020.
Tabelin, C.B., Hashimoto, A., Igarashi, T., Yoneda, T., 2014. Leaching of boron, arsenic and selenium from sedimentary rocks: II. pH dependence, speciation and mechanisms of release. Sci. Total Environ. 473, 244–253. https://doi.org/10.1016/j.scitotenv.2013.12.029, 474.
Tabelin, C.B., Sasaki, R., Igarashi, T., Park, I., Tamoto, S., Arima, T., Ito, M., Hiroyoshi, N., 2017. Simultaneous leaching of arsenite, arsenate, selenite and selenate, and their migration in tunnel-excavated sedimentary rocks: I. Column experiments under intermittent and unsaturated flow. Chemosphere 186, 558–569. https://doi.org/10.1016/j.chemosphere.2017.07.145.
Tamoto, S., Tabelin, C.B., Igarashi, T., Ito, M., Hiroyoshi, N., 2015. Short and long term release mechanisms of arsenic, selenium and boron from a tunnel-excavated sedimentary rock under in situ conditions. J. Contam. Hydrol. 175, 60–71. https://doi.org/10.1016/j.jconhyd.2015.01.003, 176.
Tessier, A., Campbell, P.G.C., Bisson, M., 1979. Sequential extraction procedure for the speciation of particulate trace metals. Anal. Chem. 51, 844–851. https://doi.org/10.1021/ac50043a017.
Wagai, R., Mayer, L.M., Kitayama, K., Shirato, Y., 2013. Association of organic matter with iron and aluminum across a range of soils determined via selective dissolution techniques coupled with dissolved nitrogen analysis. Biogeochemistry 112, 95–109. https://doi.org/10.1007/s10533-011-9652-5.
Wang, Z., Shen, X., Jing, M., Li, C., 2018. Enhanced arsenic removal from drinking water by FeOOH/γ-Al2O3 granules. J. Alloys Compd. 735, 1620–1628. https://doi.org/10.1016/j.jallcom.2017.11.284.
Wenzel, W.W., Kirchbaumer, N., Prohaska, T., Stingeder, G., Lombi, E., Adriano, D.C., 2001. Arsenic fractionation in soils using an improved sequential extraction procedure. Anal. Chim. Acta 436, 309–323. https://doi.org/10.1016/S0003-2670(01)00924-2.
Wilkin, R.T., Barnes, H.L., Brantley, S.L., 1996. The size distribution of framboidal pyrite in modern sediments: an indicator of redox conditions. Geochem. Cosmochim. Acta 60, 3897–3912. https://doi.org/10.1016/0016-7037(96)00209-8.
Wilkin, R.T., Lee, T.R., Beak, D.G., Anderson, R., Burns, B., 2018. Groundwater co-contaminant behavior of arsenic and selenium at a lead and zinc smelting facility. Appl. Geochem. 89, 255–264. https://doi.org/10.1016/j.apgeochem.2017.12.011.
Xiang, Z., Dong, L., Hongling, B., Liangliang, D., Hongmei, L., Peng, Y., Peixin, D., Hongzhe, S., 2018. XRD-based quantitative analysis of clay minerals using reference intensity ratios, mineral intensity factors, Rietveld, and full pattern summation methods: a critical review. Solid Earth Sciences 3, 16–29.
Xu, J., Ding, W., Wu, F., Mailhot, G., Zhou, D., Hanna, K., 2016. Rapid catalytic oxidation of arsenite to arsenate in an iron(III)/sulfite system under visible light. Appl. Catal. B Environ. 186, 56–61. https://doi.org/10.1016/j.apcatb.2015.12.033.
Yang, H., He, M., 2016. Distribution and speciation of selenium, antimony, and arsenic in soils and sediments around the area of xikuangshan (China): soil. Clean 44, 1538–1546. https://doi.org/10.1002/clen.201400522.
Zakharova, E.A., Noskova, G.N., Moskaleva, M.L., Elesova, E.E., Wildgoose, G.G., 2015. Investigations into the speciation of inorganic arsenic in weakly alkaline medium by voltammetry. Electroanalysis 27, 890–901. https://doi.org/10.1002/elan.201500034.
Zhang Jr., Y., W T, F., 2003. Determination of selenium fractionation and speciation in wetland sediments by parallel extraction. Int. J. Environ. Anal. Chem. 83, 315–326. https://doi.org/10.1080/0306731031000076850.